Fault and fluid interaction in a rifted margin: integrated study of calcite-sealed fault-related structures (southern Corinth margin)

A. BENEDICTO[1], V. PLAGNES[2], P. VERGÉLY[1], N. FLOTTÉ[1] & R. A. SCHULTZ[3]

[1]*Dynamics of Fault Systems Group, UMR-7072 Tectonique, Université Paris Sud XI, 91405 Orsay, France (e-mail: Antonio.Benedicto-Esteban@u-psud.fr)*

[2]*UMR-7619 Sisyphe, Université Paris VI, 75252 Paris, France*

[3]*Department of Geological Sciences and Engineering, University of Nevada, Reno, NV, USA*

Abstract: This work integrates microstructural, petrologic, microthermometric and geochemical analysis of calcite-sealed fault-related structures of the major faults of the southern margin of the Corinth rift (Greece). It draws attention to the main deformational processes and fault–fluid interaction in fault zones along the whole margin. Data analysed come from the compact breccia located immediately adjacent to major fault planes. Samples were collected at different positions alongside different faults juxtaposing synrift continental deposits (hanging wall) against the prerift Pindus limestones (footwall). This implies hectometric fault displacements and that the fault zones have recorded a relatively long evolution of deformation. Our study identifies four main deformation features common to all studied faults: calcite cemented breccia, extensional veins, shear veins and fault slip surfaces. The integrated data analysis shows that deformation structures and fault rocks that coexist in the same outcrop formed at different depths and times. During inferred upward fault propagation, the style of deformation evolved from distributed (brecciation) to localized (slip surfaces) and from a closed system with fluid–rock equilibrium during brecciation to a more open one with limited influx of meteoric water during extensional and shear fracturing. This implies relative uplift of the footwall during fault propagation and fault interaction with different water aquifers as the fault propagates upwards. The results demonstrate similar fault evolution and fault–fluid interaction through the entire rifted margin and during the whole rifting period.

The south side of the Gulf of Corinth (Greece) is a much studied area because it is one of the most seismically active areas in the Euro-Mediterranean region (see Bernard *et al.* 2006 and references therein), and it has been selected for drilling and *in situ* monitoring of an active fault (Corinth Rift Laboratory, Cornet *et al.* 2004). Currently stress, strain, chemistry of the aquifer, pore pressure, fluid flow in some aquifers and tide are being continuously monitored and recorded (Henry & Moretti 2006). One of the aims of such a drilling and monitoring project (e.g., the Nojima Fault Drilling, Lin *et al.* 2003) is to investigate fault–fluid interactions during fault activity. Understanding of fault–fluid interactions is essential to understanding fault mechanics and coseismic and interseismic faulting processes. One method to study long-lived fault–fluid interactions is by studying syntectonic mineralization within outcropping ancient fault zones (Labaume *et al.* 1991; Bradbury & Woodwell 1987; Muchez *et al.* 1995). Combined micro-structural, petrologic, microthermometric and geochemical analysis of synkinematic fault and fracture-related calcites permit the evaluation of fluid sources and flow pathways (e.g., Travé *et al.* 1998; Boles & Grivetti 2000; Cello *et al.* 2001; Pili *et al.* 2003), associated deformation mechanisms and fluid-driven mass transfers in fault zones (e.g., Travé *et al.* 1998; Sibson 2000; Labaume *et al.* 2004*a*; Micarelli *et al.*, 2005).

The exposed southern margin of the active Corinth continental rift (northern Peloponnesus) has experienced intensive uplift since rifting started (e.g., Collier *et al.* 1992; Sorel 2000; Leeder *et al.* 2003). Uplift has led to the exhumation and exposition of numerous ancient to active normal faults (Fig. 2). In a similar way to faults described in other areas of the Aegean region (Vita-Finzi & King 1985; Stewart & Hancock 1988, 1990), fault zones in the Northern-Peloponnesus area are characterized by several layers of tectonic breccia rocks and master fault slip surfaces. Breccia fault rocks and fault-related fractures are calcite-sealed, attesting to the presence of palaeofluids during deformation.

Here we combine a micro-structural and petrologic analysis (conventional, C, and cathodoluminescence, CL, microscopy) of breccia fault rocks and major fault planes with a microthermometric (fluid inclusion) and geochemical (stable isotope)

From: WIBBERLEY, C. A. J., KURZ, W., IMBER, J., HOLDSWORTH, R. E. & COLLETTINI, C. (eds) *The Internal Structure of Fault Zones: Implications for Mechanical and Fluid-Flow Properties*. **299**, 257–275.
DOI: 10.1144/SP299.16 0305-8719/08/$15.00

analysis of fault-related syn-kinematic calcite cements collected along the entire southern Corinth rifted margin. The aim is to investigate common patterns of fault and palaeofluid features during spatial–temporal fault evolution at the scale of a rifted margin. An analogous study carried out in the same region but only for a unique outcrop of secondary faults related to a major structure is that of Labaume *et al.* (2004*a*), which presents complementary results.

Geological setting

The Corinth rift is an active N110° striking asymmetric structure belonging to a system of horsts and grabens which extend from the North Anatolian fault termination in the Aegean Sea to the Kephalonia transform fault in the Ionian Sea (Fig. 1). It cuts obliquely through the Cenozoic N160° thrust belt of the external Hellenides which controls the structure of the Triassic to Oligocene prerift basement (Aubouin & Dercourt 1962; Dercourt 1964).

Different rifting models have been proposed in the last several years and these are still debated. Westaway (2002) proposed that the overall form of the Gulf of Corinth is the result of flow of plastic lower continental crust from beneath its subsiding depocentre to beneath its uplifting surroundings. Other authors propose that the rift may be controlled by a major low-angle north-dipping detachment (Sorel 2000; Exadaktylos *et al.* 2003; Flotté 2003), initiated 1.7–1.5 Ma ago (Sorel 2000; Flotté 2003). Numerical modelling by Le Pourhiet (2004) and Le Pourhiet *et al.* (2004), and field analysis by Bally (2005) suggest a deeper detachment related to the presence under the Gulf of Corinth of the inherited Phyllades metamorphic thrust sheet. Additionally, some authors have suggested that some faults such as the Eliki and Aegion faults could have formed during the uplift of the Peloponnese as an 'external' phenomenon superimposed on the opening of the Gulf of Corinth (Moretti *et al.* 2003).

Whatever rifting model is assumed (which is not essential to this paper), the fact is that a great number of normal faults crop out in the southern margin of the Gulf of Corinth (northern Peloponnesus; Fig. 2). They are responsible for south-dipping block tilting and syntectonic half-graben basin formation (Brooks & Ferentinos 1984; Ferentinos *et al.* 1985; Flotté & Sorel 2001; Exadaktylos *et al.* 2003; Sachpazi *et al.* 2003). Since initiation of rifting, normal fault activity has, in a general way, progressively migrated to the north (Seger & Alexander 1993; Sorel 2000; Goldsworthy & Jackson 2001; Flotté 2003; even if locally some faults can be 'out of sequence', see for example Causse

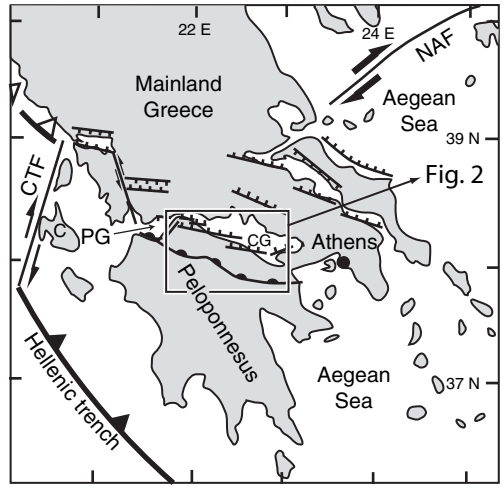

Fig. 1. Location of the Gulf of Corinth (CG) rift in the plate tectonic context. The studied area (southern margin of the rift) is squared. NAF, North Anatolian Fault; CTF, Cephalonian Transfer Fault; PG, Gulf of Patras.

et al. 2004), forming several major extensional fault systems that may be differentiated according to their relative chronostratigraphy of basin-fills (Flotté 2003). Fault activity today is located close to the present day coastline and offshore of the Gulf of Corinth (Lyon-Caen *et al.* 2004; Pi alparin *et al.* 2004).

Major extensional fault systems in the northern Peloponnesus are 20–50 km long (Fig. 2) and are orthogonal to the N10°E direction of extension measured on fault planes from striation and grooves (Flotté & Sorel 2001). Faults cross-cut the Triassic to Oligocene marine rocks forming the prerift basement, and the continental to marine Quaternary deposits associated with the rifting period. The prerift terrains are classically divided into several zones that correspond to the palaeogeographic pre-orogenic and foreland basin of the Hellenides (Dercourt 1964; Aubouin & Dercourt 1962). In the Northern Peloponnesus, three of those units are well represented (Sébrier 1977; De Wever 1975): the Phyllades or Zaroukla zone, composed of metamorphic rocks; the Gavrovo–Tripolitsa zone mainly made up of neritic and platform limestones; and the Pindus–Olonos zone, constituted by radiolarites, deep-basin limestones and flysch deposits (De Wever 1975; Dufaure 1977; Fig. 3). Those palaeogeographic domains were deformed during Hellenides folding and thrusting: the Zaroukla unit is overthrusted by the Gavrovo–Tripolitsa neritic domain which is, in turn, overthrusted by the Pindus–Olonos pelagic domain over more than 100 km (De Wever 1975).

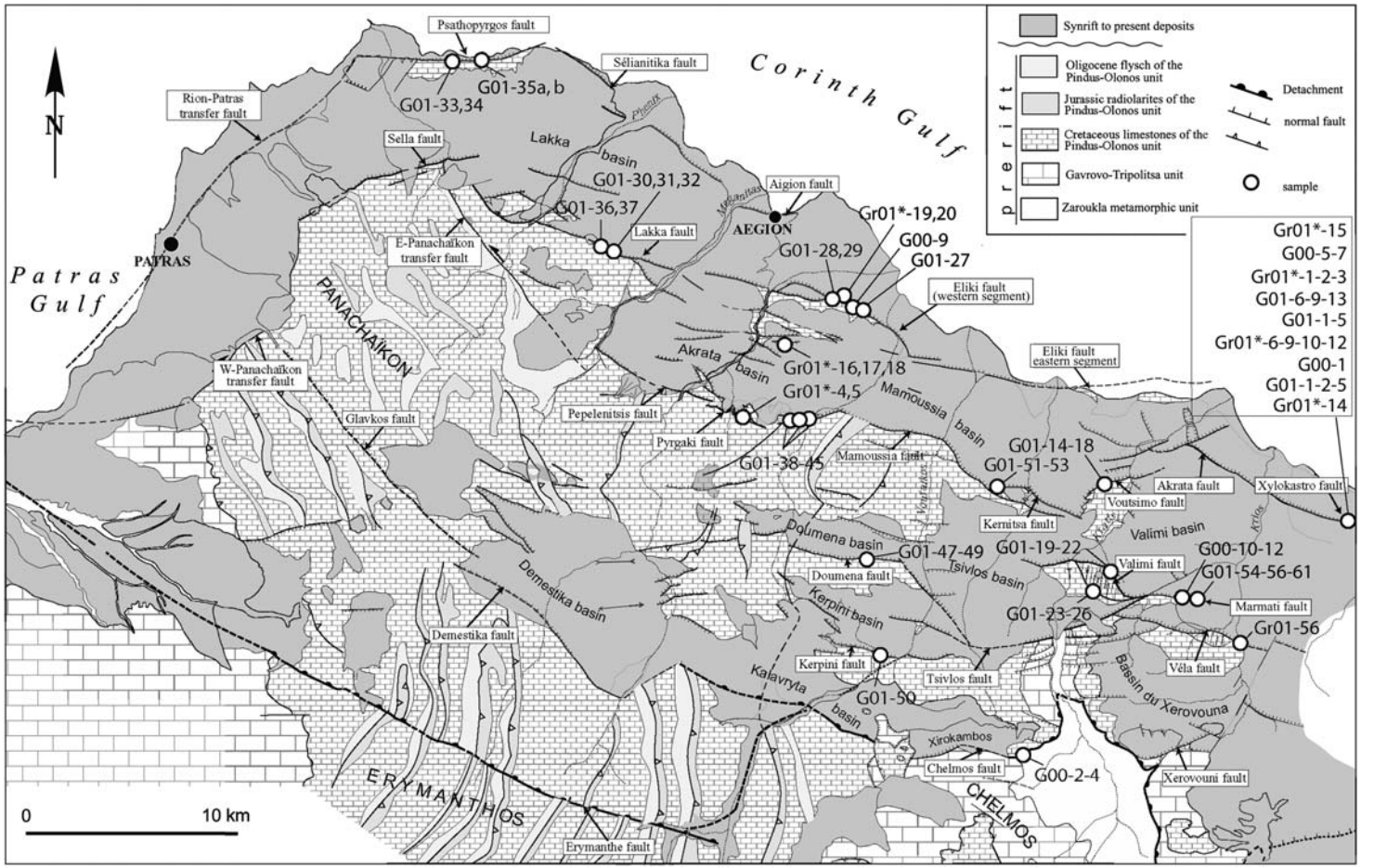

Fig. 2. Tectonic map with sample locations (modified after Flotté 2003).

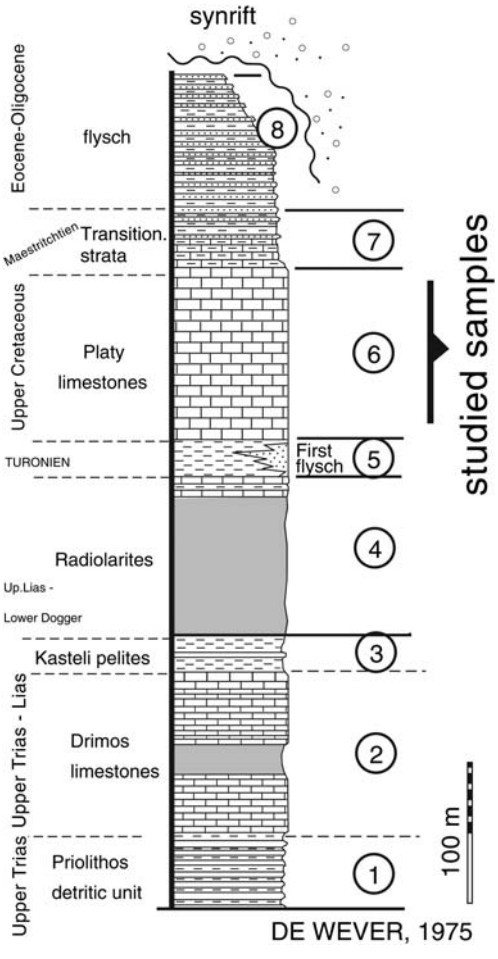

Fig. 3. Stratigraphy of the Pindus–Olonos unit described in the northern Peloponnesus by De Wever (1975). This stratigraphic series mainly forms the outcropping footwall of the studied faults. All samples come from the Upper Cretaceous Platy Limestones formation (numbered 6).

The prerift basement mainly outcrops in the footwalls of normal faults where, except in the footwall of the detachment fault, it is mainly dominated by micritic platy limestones of the Pindus–Olonos unit.

Rifting started in a continental setting and evolved to a marine one. Synrift basin-fill deposits are formed by continental marls, sands and conglomerates, and detritic marine rocks (Ori 1989; Dufaure 1975). Close to the coast, they are generally formed by coarse-grained Gilbert-type fan-deltas (Collier 1990; Seger & Alexander 1993; Dart *et al.* 1994; Malartre *et al.* 2004).

Fault zone data

The fault zones in the prerift carbonate rocks of the Aegean region were first described by Vita-Finzi & King (1985), Stewart & Hancock (1988) and Stewart & Hancock (1990), based on examples of faults located in the Gulf of Alkonides (east of the Gulf of Corinth) and in the Izmir region (Turkey). Following these authors, fault zones are characterized by (see fig. 7 in Stewart & Hancock 1988): (1) a shatter zone of dense fractures disturbing bedding of the footwall; (2) one (or several) zone-parallel layer(s) of incohesive breccia overlain by a compact breccia formed by clast supported elements in a matrix of clast fragments and secondary calcite cement (or 'stylobreccia' when highly deformation occurs); and (3) a slip surface. Breccia layers may be recurrent between several slip planes in larger fault zones.

Studies carried on the northern Peloponnesus (Flotté 2003; Micarelli *et al.* 2003; Daniel *et al.* 2004; Labaume *et al.* 2004*a*; Benedicto *et al.* 2004) also show the major occurrence of alternating cataclastic and/or breccia sheets and fault planes. Micarelli *et al.* (2003) describe the Pyrgaki, Eliki and Aegion faults (Fig. 2) as formed by a fault damage zone composed of several main and secondary fault planes with which are associated fault cores of variable thickness mainly formed by cemented breccia, cohesive cataclasite and/or incohesive gouge, with random or locally foliated fabrics (foliated cataclasites). Clay shearing (Daniel *et al.* 2004; Benedicto *et al.* 2004) and calcite-cemented fractures (Labaume *et al.* 2004*a*) are also representative features.

The common structure of major outcropping faults observed in the northern Peloponnesus may be characterized by a deformed footwall mainly composed of micritic platy limestones of the Pindus–Olonos unit (Pindus Limestones), a fault-parallel zone in which the limestones are partially fractured (shatter zone of Stewart & Hancock 1990) and a zone of compact calcite cemented breccia underlain major, well-exposed, huge slip planes of pure normal motion (Fig. 4). This brecciated fault core constitutes a zone of variable thickness with abundant secondary slip planes locally containing 'pull-apart' synkinematic striated calcite structures (Fig. 5). Locally, non-cohesive breccias (not calcite cemented) may also be present. Further detailed description of several fault zones may be found in Micarelli *et al.* (2003), Daniel *et al.* (2004), Labaume *et al.* (2004*a*) and Benedicto *et al.* (2004).

Data analysed in this paper correspond to the compact breccia immediately located beneath major fault slip surfaces (i.e., compact breccia of Stewart & Hancock 1988 and fault core of Micarelli

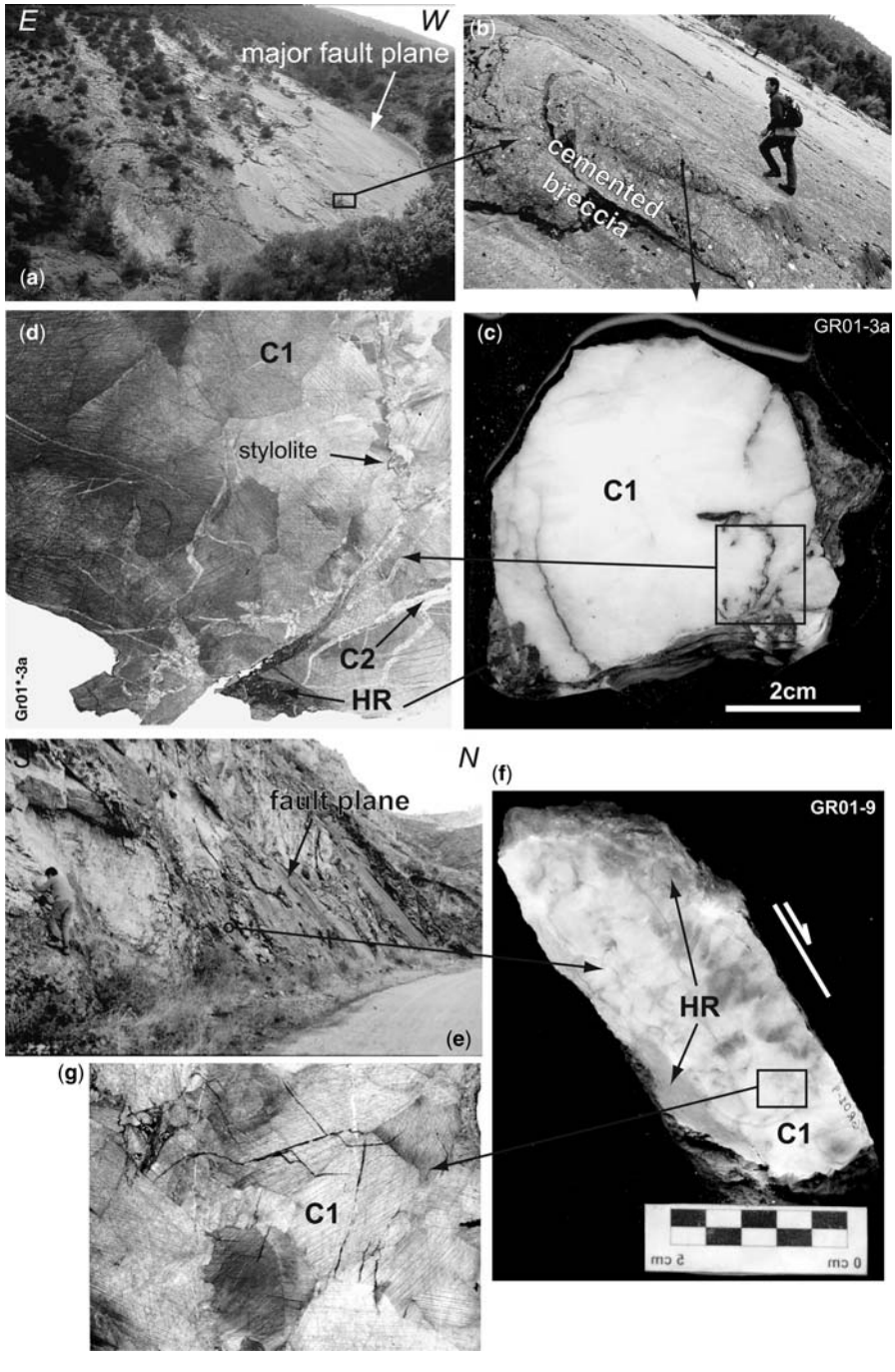

Fig. 4. The Xylokastro fault. (**a**) View of the major fault plane. (**b**) Detail of the cemented breccia underlying the major fault plane. (**c**) Cut sample GR01-3a. (**d**) Thin section viewed under conventional optical microscopy. (**e**) View of the upper part of the Xylokastro fault. (**f**) Cut sample GR01–9. (**g**) Thin section viewed under optical microscopy. C1, calcite cement type 1; C2, calcite cement type 2; HR = host limestone fragment.

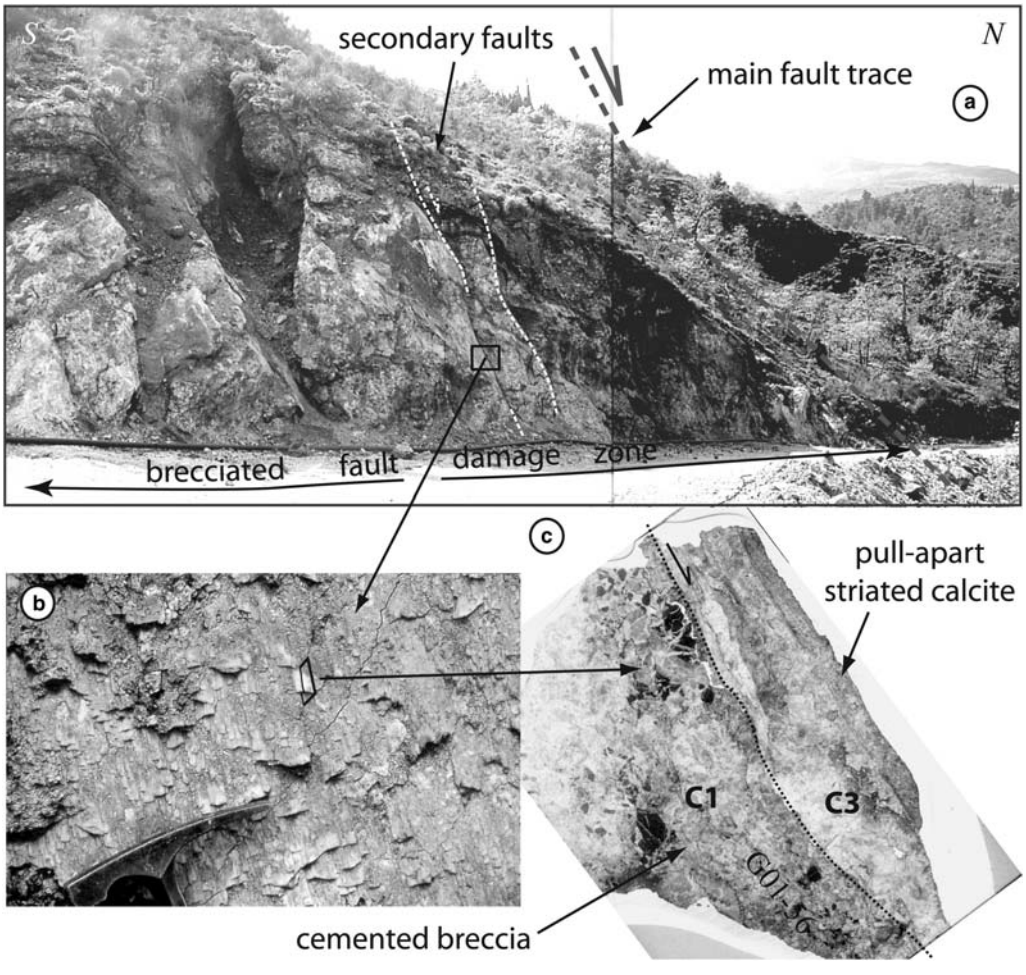

Fig. 5. The Vela fault. (**a**) Picture showing the brecciated damage fault zone cut through by secondary faults. (**b**) Detail of a secondary fault plane with 'pull-apart' syn-kinematic striated calcite. (**c**) Thin section of the sample G01–56.

et al. 2003). Samples were collected at different positions alongside (vertical and horizontal) different faults (Fig. 2). From time to time, slip surfaces are locally sealed by a post-kinematic (karst-type) calcite. For comparison with synkinematic calcites, we also analysed this post-kinematic type. All samples discussed in this paper come from fault zones juxtaposing synrift continental detritic deposits of the hanging wall (presently partially eroded) to the prerift Pindus limestones of the footwall. This implies hectometre fault displacements and that the fault zones analysed have recorded a long fault evolution.

A conventional microstructural and petrologic analysis coupled with a cathodoluminescence analysis was carried out on more than 30 thin sections from 93 samples collected on different faults (Fig. 2). Geochemical analysis for stable isotopes ($\delta^{18}O$ and $\delta^{13}C$) was performed on 31 samples and fluid inclusions for thermometric analysis were investigated in 10 samples.

Microstructural and petrologic analysis

Extensional deformation recorded in the compact breccia is consistently marked by: (i) calcite-cemented breccia (Fig. 6b); (ii) extensional calcite-sealed veins (Fig. 6b); (iii) shear calcite-sealed veins (Fig. 6b); and (iv) stylolites (Fig. 4d). Although stylolite features are abundant and can accommodate large amounts of extensional deformation (Labaume *et al.* 2004*b*; Benedicto *et al.* 2004), here we only focus on the synkinematic

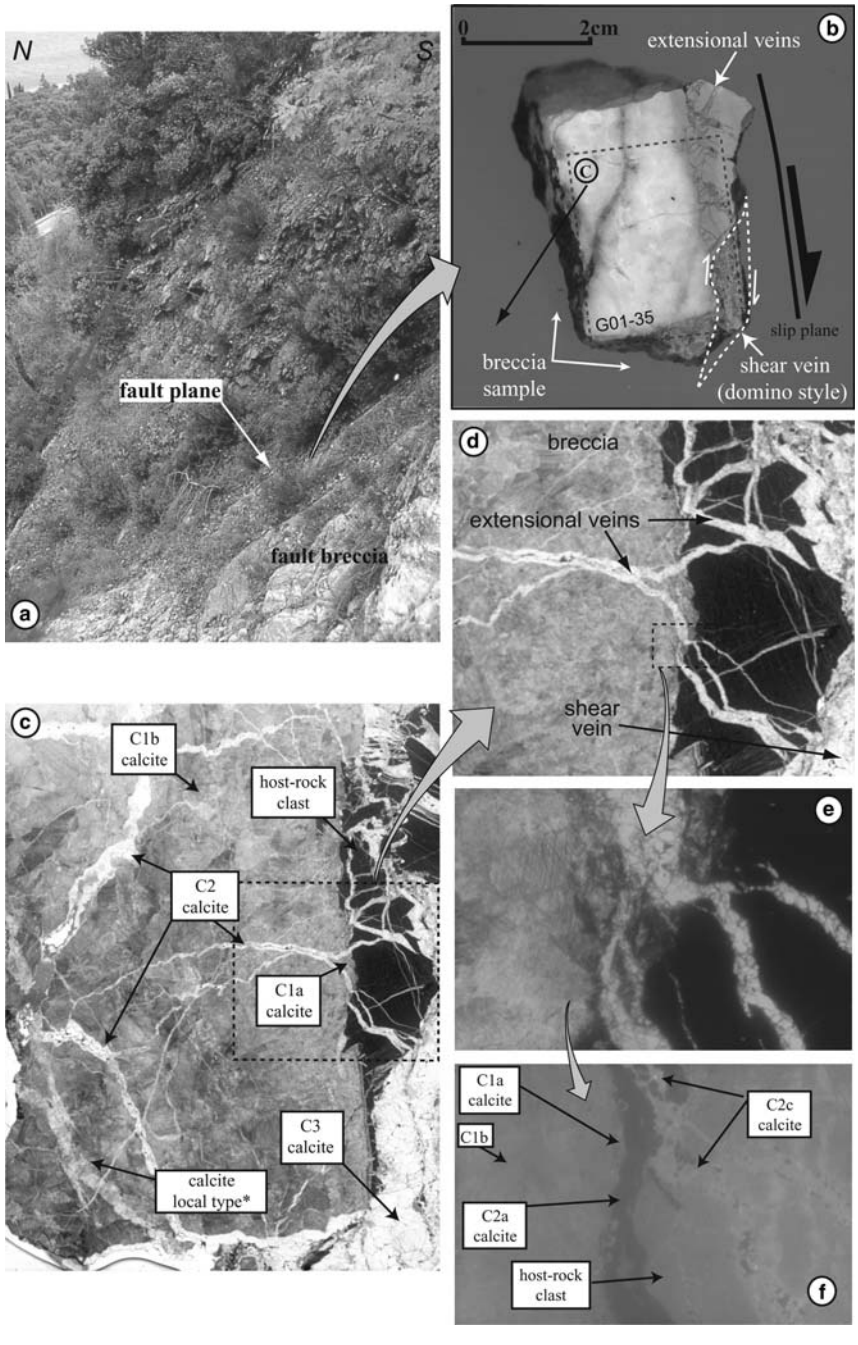

Fig. 6. (**a**) The Psatopyrgos fault. (**b**) Cut sample G01–35. (**c**) & (**d**) Thin section viewed under optical microscopy. Calcite cement types are indicated. (**e**) & (**f**) Zoom on thin section viewed under cathodoluminescence microscopy.

calcite-sealed structures which appear better organized, show clearer cross-cutting relationships and contain information about palaeofluids involved during deformation. This also avoids misinterpretation of stylolites that could be associated with the inherited compressional deformation (Daniel *et al.* 2004). We synthesize the dominant and common deformation and calcite cementation features repeatedly observed along the studied faults and illustrate them with the most characteristic samples.

The microscopy analysis (both optical and cathodoluminescence) reveals: (a) two types of calcite breccia cements; (b) one dominant random network of extensional calcite veins; and (c) one type of shear calcite veins.

Calcite breccia cements (C1)

The host-micrite limestone clasts involved within the breccia are cemented by a rim, very often imperceptible, of micro-sparitic calcite immediately surrounding the clasts, separated from the host-limestone clasts by a vague boundary (C1a in Fig. 6b). When the clasts are slightly disaggregated, this cement may completely fill up the spaces between them (Fig. 7c & d, depicted in light grey). When the clasts are strongly disaggregated, this cement type passes rapidly, but progressively, to sparitic calcite cement with large crystals, anhedral–subhedral, highly twinned and fractured (C1b in Figs 6c & 7d). CL microscopy shows that both types of cements have the same red-orange luminescence as the host-limestone (Figs 6e & 7g). The location of the micro-sparitic cement adjacent to the host-limestone clasts, and its indistinct boundary, suggest that this cement precedes formation of the sparitic one (i.e., associated with early stages of brecciation and cementation). The cementation process seems to be continuous (progressive transition) from the micro-sparitic (C1a) to the sparitic calcite (C1b).

Extensional calcite veins (C2)

Host-limestone clasts and calcite breccia cements are cross-cut by a random network of irregular, thin veins filled by sparitic calcite (Fig. 6b), with small crystals, anhedral–subhedral, few or not twinned and/or fractured (C2 in Figs 6c & 7e). Often, small, darker, twinned calcite crystals can be observed at the centre of the veins (Fig. 7c).

This type of vein is characterized in cathodolum inescence microscopy by a dark red or weakly luminescent calcite (C2a in Figs 6f & 7g), with sometimes a darker central rim (C2b in Fig. 6f) and, occasionally, bright orange luminescent calcite disseminated more or less along the centre of the veins (C2c in Figs 6f & 7g). The spatial relationship between the few luminescent and the bright orange luminescent calcite is not clear. Sometimes the bright orange calcite appears disseminated within the weakly luminescent calcite in the same vein (Fig. 6f); other times it appears mostly filling up the major part of the vein with very few observable patches of the weakly luminescent calcite (Fig. 7g). In all the cases, boundaries between both calcite types are misty. These extensional calcite veins cross-cut and postdate C1 calcite cements.

Shear calcite veins (C3)

Shear calcite veins are present as variably sized, localized, white calcite in domino or 'pull-apart' style structures, located very close to major fault planes (C3 in Figs 6b & 8a) or appear as 'pull-apart' striated calcite on secondary fault planes (Fig. 5b & c). They are composed of three types of calcite crystals: a sometimes visible outer (border) more or less continuous rim of anhedral–subhedral small crystals, a predominant inner zone of large euhedral–subhedral, elongate, twinned calcite crystals arranged orthogonal to the veins boundaries, and a central zone of smaller subhedral crystals (Fig. 8b & c).

This calcite type has the same red-orange luminescence, darker than the C1 cements, but brighter than the C2 calcite type. Sometimes, very thin zones of brighter luminescence may be observed between the elongate crystals (which may be due to recrystallization; Fig. 8e).

In the studied samples, shear calcite veins cross-cut the host-limestone clasts and the C1 cements (Figs 6b & 8b), often underlined by stylolites (Fig. 8b). They also cross-cut the C2 extensional calcite veins, indicating a younger chronology (Fig. 6b), so we call this calcite type C3.

Post-kinematic calcite (Cp)

Clearly younger than all the syn-kinematic calcites described above is crystalline, laminate post-kinematic calcite which may be found locally draping fault slip surfaces (e.g., sample G00-1, from the Xylokastro fault, see description in Flotté *et al.* 2001). We call this calcite type Cp. This calcite type has a special interest for the interpretation of the stable isotopes.

Figure 9 depicts schematically the described microstructures, their petrologic characteristics and their cross-cutting relationships.

Stable isotopes

$\delta^{18}O$ and $\delta^{13}C$ isotope analysis allows characterization of the isotopic signature of fault-related calcites and discussion of the origin of the fluid from which those calcites formed (e.g., Travé *et al.* 1998; Boles & Grivetti 2000; Pili *et al.* 2003).

The three types of synkinematic calcites (C1, C2 and C3) were analysed (via micro-sampling by using a dental drill), plus the host-limestone and the post-kinematic calcite (Cp). Thirty-one from 93 collected samples were analysed for both C and O isotope ratios using a VG Optima mass

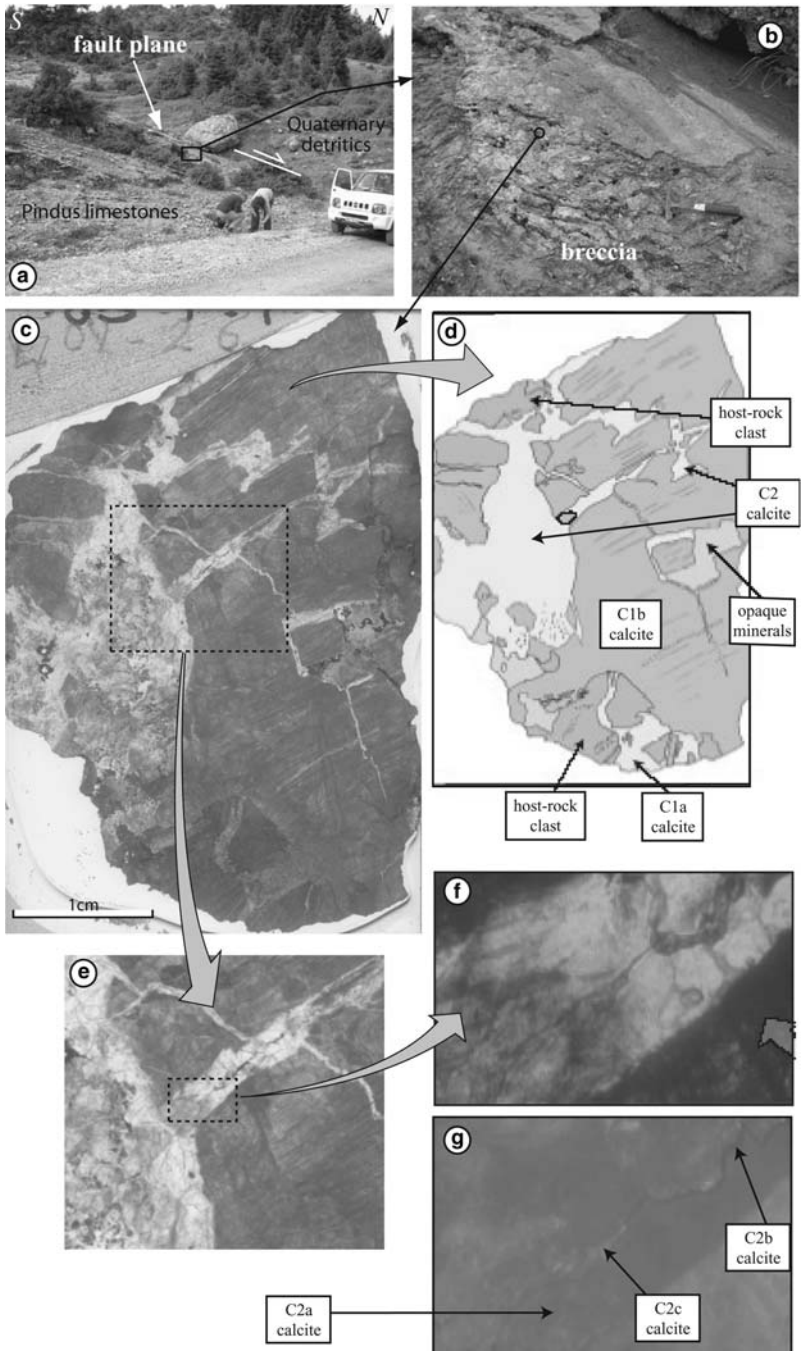

Fig. 7. (**a**) & (**b**) The Valimi fault and the brecciated fault core. (**c**) Thin section of sample G01-26 viewed under optical microscopy. (**d**) Synthetic sketch showing different calcite types. (**e**) Zoom on thin section. (**f**) & (**g**) Zoom on thin section viewed under the cathodoluminescence microscopy.

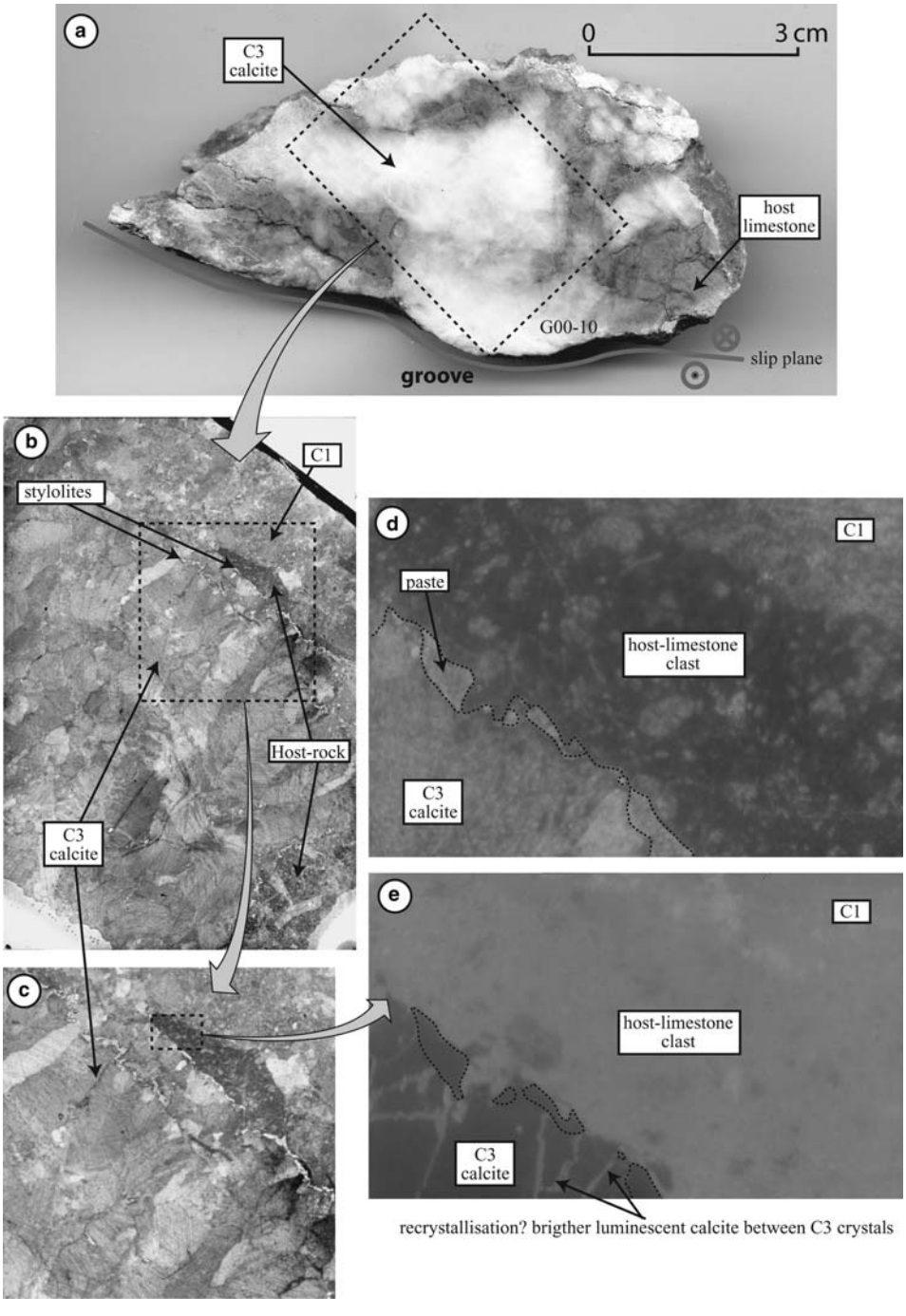

Fig. 8. (**a**) Cut sample G00-10 (from the Valimi fault). (**b**) Thin section viewed under optical microscopy. (**c**) Calcite cement types are indicated. (**d**) & (**e**) Zoom on thin section viewed under cathodoluminescence microscopy.

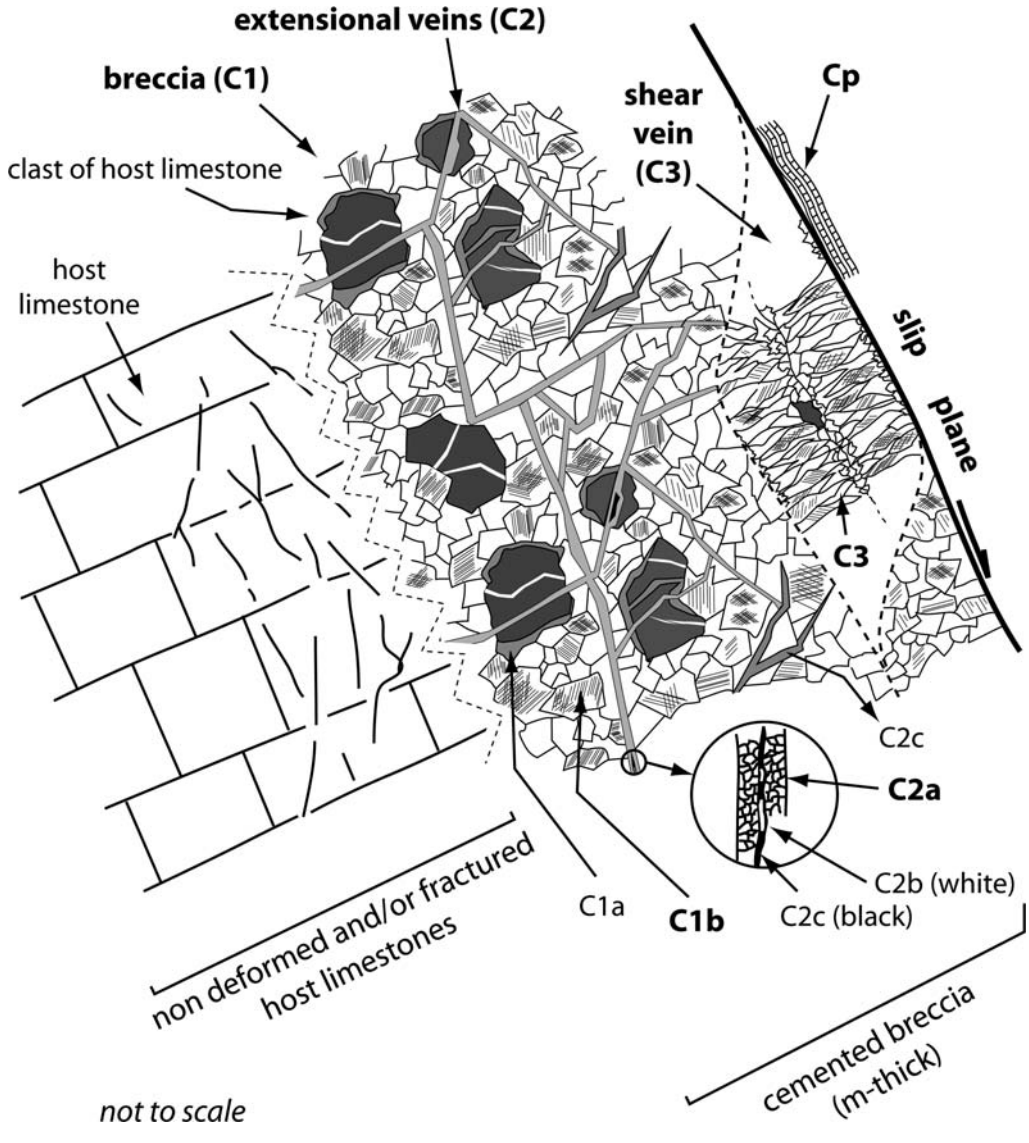

Fig. 9. Synthetic sketch showing the main microstructural and petrological patterns of the fault related calcite sealed structures (breccia with C1 cements, extensional veins with C2 cements, shear veins with C3 cement, and the main slip plane). The sketch shows their cross-cutting relationships.

spectrometer (at the LSCE[3]) after orthophosphoric acid reaction at 90 °C. The data v. PDB (PD Belemnite) have an analytical error of 0.04 and 0.06‰, respectively, for C and O.

Although usable data obtained are reduced in number (25 samples from 31, Fig. 10), values are consistent with microstructural and petrological data and demonstrate that each calcite type is different. Figure 10 shows data plotted in a $\delta^{18}O$ v. $\delta^{13}C$ graph. Although in this paper we mainly focus on the meaning of $\delta^{18}O$ values, the combined plot of $\delta^{18}O$ and $\delta^{13}C$ isotopes allows us to better distinguish the different fields in which the data group. The $\delta^{18}O$ values of the bulk-rock range from -2.1 to -3.1‰ PDB, a range which also corresponds to values of the C1 calcite type (-1.1 to -5.1‰ PDB). The C2 calcite type presents values ranging from -11 to -12 ‰ PDB, the C3

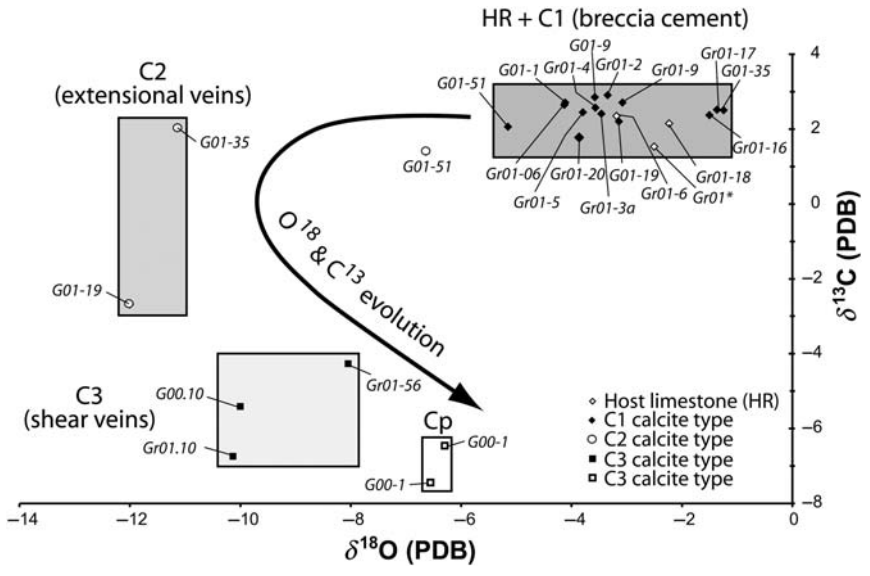

Fig. 10. Plot of values of $\delta^{18}O$ v. $\delta^{13}C$ (calcite in ‰ PDB). The graph shows the characteristic signature of each type of calcite C1, C2, C3, Cp and the host limestone. The syn-kinematic calcite signature evolves from equilibrated with the host limestones for the C1 (breccia cement) towards values of $\delta^{18}O$ in disequilibrium with the host-rock (C2, extensional and C3, shear veins) and progressively closer to that of the post-kinematic karstic-type calcites (Cp).

calcite type has values from −8.5 to −10.1‰ PDB, and the Cp post-kinematic calcite shows values around −6.3‰ PDB. The synkinematic calcite signature evolves from equilibrated with the host limestones for the C1 towards values in $\delta^{18}O$ in disequilibrium with the host-rock and progressively closer to that of the post-kinematic karstic-type calcite (Cp).

Thermometry data

Fluid inclusions were analysed (Université Paris VI-UMR Sisyphe and XI-UMR Orsayterre) in order to estimate palaeo-temperatures of calcite precipitation. Fluid inclusions are rare in the fault-related calcites of the southern margin of the Corinth rift and are difficult to analyse, allowing only a qualitative, but nevertheless helpful, interpretation.

In the C1 calcite cement type (breccia cement), most fluid inclusions are single phase and water filled, suggesting formation (or recrystallisation) at temperatures lower than 60 °C (Roedder 1984; Goldstein & Reynolds 1994). Mono-phase fluid inclusions display homogeneous freezing temperatures (T_{fg}) around −12 °C (Fig. 11). This indicates salinities of NaCl wt% equivalent ≈16 (Bodnar 1993), suggesting relatively 'salty' water (Fig. 11). A few biphasic inclusions were also found within the C1 calcite type. These inclusions systematically disappeared very soon when heating over 40 °C, without coming back upon cooling, indicating a meta-stable state. A confident two-phase inclusion identification comes from the Vela fault (sample G01-56 indicated with a start in Fig. 11). It displays a homogenization temperature (T_h) of 56 °C and a freezing temperature of −12 °C. This freezing temperature, which is exactly the same as that of the one-phase fluid inclusions, indicates a similar formation temperature for the observed one-phase inclusions. Biphasic inclusions have also been observed in samples from the Pyrgaki fault (L. Micarelli, pers. com).

In the C2 calcite type (extensional veins) only one-phase fluid inclusions were found. This fact and the lack of two-phase inclusions suggest formation temperatures lower than 50 °C. Single-phase, water-filled inclusions display homogeneous freezing temperatures around −2 °C (Fig. 11), indicating salinities of NaCl% wt equivalent <4 (Bodnar 1993), lower than that of the two-phase fluid inclusions in C1.

In C3 calcite type (shear veins) very few and localized one-phase inclusions were observed. The lack of fluid inclusions can be attributed to a very low formation temperature or to fluid leakage due to twinning and fracturing during shearing. This latter phenomenon could also explain the poor set of two-phase fluid inclusions 'conserved' in the

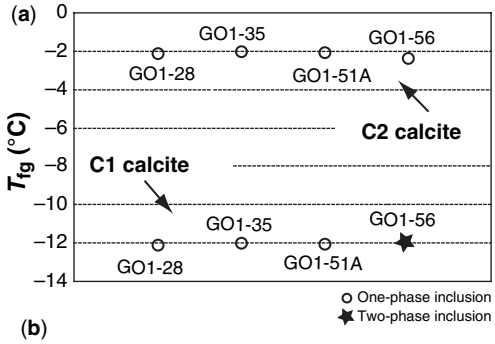

(b)

Sample	C1 calcite T_{fg} (°C)	C2 calcite T_{fg} (°C)
GO1-28	–12.2	–2.2
GO1-35	–12.1	–2.1
GO1-51A	–12.1	–2.1
GO1-56	–12.0	–2.4
	–12.1	–2.2
Salinity (equiv. NaCl%)	16.05	3.71

Fig. 11. Graph and table showing data from fluid inclusions analysis. Note the homogeneous freezing temperature (T_{fg}) of one- and two-phase inclusions observed in the C1 calcite type, and those of the one-phase inclusions observed in the C2 calcite type.

C1 calcite type. Note that C1 and C3 calcites are twinned, while the C2 type is rarely twinned.

Thermometry data suggest that cement calcite type C1 could crystallize at temperatures around/or over 50 °C, corresponding to the minimum temperature required for the genesis of two-phase inclusions in calcite (Roedder 1984; Goldstein & Reynolds 1994). Assuming a normal geothermal gradient of 30 °C km^{-1} and an average surface temperature of 15 °C, this calcite type could form at 1000–1200 m depth. C2 and C3 calcite types should precipitate at shallower depth where temperatures are lower than 50 °C.

Integrated data interpretation

The microstructural and petrologic analysis reveals three types of syn-kinematic calcites (Table 1): breccia cements (C1), calcite-filling extensional veins (C2) and calcite-filling shear veins (C3). Their chronology is determined by cross-cutting relationships. C1 cements are the first generation of calcite. C1 cements are cross-cut by the C2 extensional veins filled by a second generation of calcite. The shear veins filled by the C3 calcite cross-cut C1 and C2, thus post-dating them. C3 constitutes a third generation of calcite. This C3 calcite also forms the 'pull-apart' synkinematic striated structures of secondary faults that cross-cut the compact breccia. All these calcite-filled structures are cross-cut by the large slip surfaces that form the major fault scarps. Fault slip surfaces can in turn be draped by the post-kinematic Gp calcite which constitutes a fourth generation of calcite.

Cathodoluminescence microscopy also suggests that the three generations of calcite are different (Table 1), which is probably related to three main different types of fluids interacting with the faults (at least related to the Fe and Mn composition). We neglect the nuances of C2b and C2c because they appear in very small amounts inside the major C2a type, and are also difficult to analyse and to interpret unambiguously. In a noteworthy way, the C1 (breccia cement) has the same red-orange luminescence as the host-limestone, suggesting fluid probably in chemical equilibrium with the latter. The younger C2 and C3 have different luminescence than the host limestone, suggesting fluid in chemical disequilibrium. Differences of CL between C2 and C3 also indicate different fluid composition for each generation.

$\delta^{18}O$ and $\delta^{13}C$ isotope values (Fig. 10 and Table 1) indicate origins from different fluid (water) types for each generation of calcite: the HR and the C1 show similar values of $\delta^{18}O$ and $\delta^{13}C$. The $\delta^{18}O$ values of the HR are lower than reported for the Cretaceous rocks of marine origin (Pirrie & Marshall 1990), suggesting diagenetic

Table 1. *Synthesis of the calcite types and generations, cathodoluminescence and $\delta^{18}O$ data*

Calcite type		CL	Fluid Inclusions	$\delta^{18}O$(‰ v. PDB)
Host-rock in breccia	HR		—	between −2.1 and −3.1
Cements (generation 1)	C1a	Red-orange	Biphasic, $T > 50$ °C	between −1.1 and −5.1
	C1b			
Extensional veins (generation 2)	C2a	Dark-red	Monophasic, $T < 50$ °C	between −11 and −12
	C2b	Dark	—	—
	C2c	Bright orange	—	—
Shear veins (generation 3)	C3	Red-orange	Monophasic, $T < 50$ °C?	between −8.5 and −10.1
Post-kinematic (generation 4)	Gp		No	around −6.3

alteration of the carbonates in shallow meteoric and/or burial conditions (Travé *et al.* 1998). The salinity of two-phase fluid inclusions within C1 is quite elevated (NaCl% wt equivalent = 16), perhaps implying a marine water origin influenced by evaporation. In fact, this value of salinity is higher than that of marine water. Nevertheless, a strong meteoric water influence is suggested by the low Sr content (1200 ppm, see Labaume *et al.* 2004*b*), and the clearly positive values of $\delta^{13}C$ that are characteristic of meteoric water. A meteoric water influence may additionally be inferred from the observation that the Pindus limestones were exhumed and exposed to a near-surface environment during the Cerozoic Hellenides orogeny, which structured the prerift basement (Dercourt 1964; Aubouin & Dercourt 1962). Moreover, for a similar fluid, the O isotope values can shift to higher values when the water–rock ratio decreases (Craig *et al.* 1956) in contexts of impermeable rocks or sedimentary rocks where fluid flooding is restricted, as may be the case for the Pindus limestones. The origin of the fluid of C1 calcite remains uncertain. Nevertheless, the fact is that $\delta^{13}C$ values (Fig. 10) confirm water in equilibrium with the hosting limestone, consistent with the independent cathodoluminescence data. This indicates a closed hydrological and chemical system during fault-related breccia sealing. Metastable two-phase fluid inclusions indicate breccia cementation (inferred as breccia formation) at a maximum temperature of 55 °C, most probably between 40 and 55 °C.

Figure 12 shows the plot of $\delta^{18}O$-calcite values (in PDB) v. $\delta^{18}O$-fluid (values in SMOW) as a function of the temperature fields diagram [$T = f(\delta^{18}O_{fluid})$]. Groundwater data come from Pizzino *et al.* (2004). Values range between −6 and −9.4‰ SMOW. Isotopic data of meteoric water comes from the GNIP website for Athens (www-naweb.iaea.org/napc/ih/GNIP/IHS_GNIP.html). In order to correct for the influence of the different altitude between the recharge zone in Athens (near sea-level) and in the northern Peloponnesus (*c.* 2000 m), a *c.* 2000 m elevation correction was applied. The extrapolated value to the northern Peloponnesus $\delta^{18}O$ of meteoric recharge then ranges from −5 to −10‰ SMOW.

In the C2 (calcite in extensional veins), the lack of two-phase fluid inclusions indicates that calcite precipitated at temperatures lower than those established for the C1, namely lower than 40 °C (Fig. 12). Taking into account this range of temperature, the $\delta^{18}O$ isotope values (Fig. 10) indicate fluid provenance from meteoric water (Fig. 12). This is consistent with the $\delta^{13}C$ values (Fig. 10), indicating water in disequilibrium with the host limestone during extensional fracturing and sealing. The probable meteoric origin of C2 calcite can also explain the lower salinity of the one-phase fluid inclusions (NaCl wt% equivalent = 4). Nevertheless, this salinity remains quite elevated, suggesting

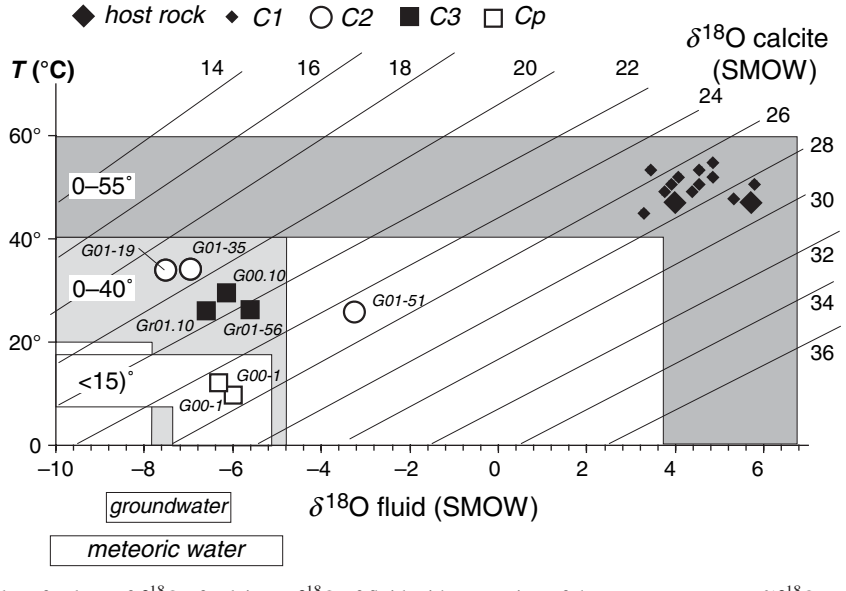

Fig. 12. Plot of values of $\delta^{18}O$ of calcite v. $\delta^{18}O$ of fluid with correction of the temperature, $T = f(\delta^{18}O_{fluid})$. The O isotope composition is interpreted by using the crystallization temperatures estimated from fluid inclusions and the isotopic fractionation coefficients of Kim & O'Neil (1997).

either significant evaporation or mixing with a more saline fluid from previous episodes (e.g., remaining C1-type fluid).

An equivalent result is found for C3 (calcite-filling shear fractures) that does not host fluid inclusions and displays values of δ^{18}O-fluid (Fig. 12), also indicating formation from meteoric water. As C3 always post-dates (cross-cuts) C2, we infer similar or lower temperatures during this calcite precipitation, probably under 30 °C. Different CL colour than C2 could suggest little variation in the composition of water. We infer that C4 (Cp) formed under near-surface conditions, at temperatures around 10–15 °C, recording the more recent palaeowater characteristics of δ^{18}O, very close to those of rain water (Fig. 12).

Concerning the ^{13}C isotopic compositions, Figure 10 shows that the C1 and the HR present a homogeneous carbon isotopic composition, clearly indicating that the fluid was equilibrated with the host limestone (Morse & Mackenzie 1990; Clark & Fritz 1997). By contrast, C2 veins exhibit more heterogeneous δ^{13}C, and C3 and C4 present clearly negative values, indicating an increasing disequilibrium with the host rock.

Faulting and fluid–rock interaction in the fault zone

Labaume *et al.* (2004*a*) studied a secondary fault set related to the Pyrgaki fault (see location in Fig. 2) and located some tens of metres north of the major fault plane, at the Taxarchion outcrop (Labaume *et al.* 2004*a*, *b*; Benedicto *et al.* 2004). They propose a model of fault zone development related to the upward propagation of a normal fault tip, derived from the model proposed by Stewart & Hancock (1988, 1990). They suggest that the central part of the fault develops with a tendency of deformation concentration from distributed stylolites and veins at the fault tip through disconnected then connected slip surfaces, attrition breccia and eventually formation of a large-scale discrete slip surface within the breccia. Our integrated microstructural, petrologic, palaeothermal and isotopic study of major faults through the entire margin supports this model and additionally suggests that deformational mechanisms organize spatially and temporally during upward fault propagation.

The first deformation mechanism occurring in the studied fault zones was random brecciation, sealed by the C1 cement. This occurred in a more or less wide zone of distributed deformation and, as suggested by fluid inclusions, at a temperature around 55 °C, that is, equivalent to a depth of around 1300 m. The cathodoluminescence and the isotopic signature of calcite cements show that this deformation occurred in a closed system with the fluid and the host rock in equilibrium. Accordingly, brecciation occurred at a minimum depth beyond the influence of the meteoric flooding water. This implies that during brecciation any external fluid flowed through the breccia corridor. This distributed deformation may be related to hydraulic extension fractures developed under a hydrostatic regime before the development of the through-going fault (Sibson 2000). Brecciation most probably occurred ahead of (above) the fault tip and breccia corridors (in the sense of Labaume *et al.*, 2004*a*) served as the initiation sites for the propagating fault through kink folding of the carbonate sequence above the fault (e.g., Johnson & Fletcher 1994).

As the C1 cement seals the breccia everywhere along the fault, it represents a potentially large volume of saturated fluid that could interact with the fault. Although the precipitation of calcite is very sensitive to the fluid saturation, the chemical fluid composition, the flow velocity, the fluid pressure and the fluid–rock ratio, Morse & Mackenzie (1993) and Lee *et al.* (1996) showed by experimental modelling that an extremely large volume of supersaturated water (i.e., 20 000 l) is required to pass through a vein (i.e., 2 mm wide, 10 cm high and 100 cm long) in order to eventually fill it with calcite. As the fault breccia is in general wider than several metres and is present all along (vertical and lateral) the fault zones, enormous quantities of flooding water would be necessary to seal it with calcite, the water coming from deeper, shallower or lateral areas. In such a case, rather than a homogeneous cement, as the C1 is, different types of calcite cements should be found, with different cathodoluminescent and geochemical signatures, in disequilibrium with the host limestone in which calcite crystallizes. This suggests that the water was rather stable in an aquifer at a given depth, and that fault–fluid interaction occurred when the fault propagated through this aquifer. Mass transfer from the host rock to the fault breccia most probably occurred by local dissolution and diffusion during micro-fracturing (see Renard *et al.* 2000) without significant water drainage (flooding) through or along the fault zone.

The second type of deformation is the small, discrete extensional fracturing that overprints the breccia and is sealed by the C2 calcite. Thermometric data indicate that this deformation pattern formed in a shallower zone than the breccia. Cathodoluminescence and isotopic signatures indicate that it occurred under the influence of meteoric water flooding (corresponding to an open system). Note that the extensional veins overprint the calcite-sealed breccia but they never contain the C1

cement; in contrast, the breccia is never cemented by the C2 calcite type. This attests to diachronous timing and/or spatial location of both deformational processes: brecciation should occur deeper than extensional fracturing. Shallower conditions during extensional fracturing must then be related not to the upward propagation of the fault tip itself but to the uplift of the whole fault zone (or footwall fault zone). Uplift may be explained by regional exhumation (i.e., Collier *et al.* 1992; Roberts & Stewart 1994; Dia *et al.* 1997; Sorel 2000; Leeder *et al.* 2003) and/or denudation of the overhead prerift and synrift series. Uplift of the fault zone of several hundred metres is then accompanied by a significant change of the mode of deformation from distributed (brecciation) to more localized extensional fracturing as suggested by Labaume *et al.* (2004*a*, *b*). This strain localization could be induced during footwall exposure by both cooler conditions and a decreasing vertical overburden stress σ_1 and a decreasing stress ratio σ_1'/σ_3' as the erosion cuts the top of the footwall and the hanging wall moves down.

The facts that (i) the C1 and C2 cements are not mixed either within the breccia or within the extensional veins, and that (ii) the C1 cement formed in a closed system (inferred at depth), emphasize that both deformational processes actually observed together in the same location must happened sequentially. Effectively, in shallower conditions where (and when) discrete extensional fracturing occurs, brecciation does not, and conversely, at depth, where brecciation occurs, discrete extensional fracturing does not.

As strain localizes along what is now the weakened fault zone, discrete shear surfaces, veins and calcite-filled 'pull-aparts' develop, overprinting and cross-cutting the breccia and the extensional veins formed previously. As deformation increases, shear structures such as the 'pull-aparts' progressively connect by short slip planes (secondary faults). This stage of deformation is equivalent to formation of a zone of gouge within which shear strains begin to localize (e.g., Bartlett *et al.* 1981; Mair & Marone 1999). Note again that the cathodoluminescent and isotopic signatures of the C3 (shear fractures cement) differ from those of the C1 and C2, and they never appear mixed in the same microstructure. Stable isotopes of C3 cement indicate a fluid closer to the signature of post-tectonic calcites (Cp) or present groundwater (see Figs 10 & 12). This suggests again diachronous timing of development related to the C1 and C2. This 'third' stage of deformation is confirmed by cross-cutting relationships between breccia, extensional and shear veins.

During upward fault propagation and progressive uplift, the fault reached and propagated through successively more shallow aquifers, trapping palaeowater present in each aquifer into the extensional (C2) and shear (C3) fractures. Note that extensional fractures are homogeneously distributed through the breccia but they are few, dense and very thin; shear veins are relatively thin and localized. Compared with the quantity of fluid necessary to form the abundant breccia cement, the relative volume of water interacting to seal extensional and shear fractures had to have been relatively small. Even in the case in which water could flow through or along the fault zone, this should represent only modest quantities.

The final stage in the faulting process is represented by the growth and emergence of the propagating fault formed by link-up of the smaller shearing fractures and short slip surfaces discussed in stage 3. At this stage, fault motion is mainly concentrated along these rough fault surfaces that progressively become the large fault escarpments outcropping at the present day. From this moment, strain and deformation are entirely concentrated along the major fault plane and displacement can increase while inducing little deformation in the surrounding areas. This could explain why the C3 calcite in the shear fractures is twinned while the C2 calcite is not.

Conclusions

This work integrates microstructural, petrologic, microthermometric and geochemical studies of calcite-sealed fault-related structures of major faults of the offshore southern margin of the Corinth rift. Results show the homogeneity through the entire margin and during the rifting period of (i) main deformational processes and fault zone evolution, and (ii) fluid–rock interaction in fault zones. It points out four main deformation patterns common to all studied faults in which large slip (fault) surfaces and related cohesive breccias are present. These are: calcite-cemented breccia, extensional veins, shear veins and fault slip surfaces. Cross-cutting relationships indicate that the breccia formed first, the extensional veins second, the shear veins third and the slip planes fourth. It occurred in progressively shallower conditions during upward fault propagation and regional uplift.

Fault zones started to develop by forming random brecciation corridors (hydraulic extension fractures). This stage represents one of distributed deformation. Calcite breccia cements, chemically equilibrated with the host limestones, indicate that at this state deformation occurred in a closed fluid–rock system. During footwall uplift and unloading by regional exhumation and/or erosion, cooler conditions, plus a decreasing vertical σ_1

and stress ratio σ_1'/σ_3' as the top of the footwall is denuded and the hanging wall moves downwards, strain localization was induced and deformation concentrated on extensional veins and shear veins respectively. Calcite cements of extensional and shear veins, in respectively higher disequilibrium with the host limestones, indicate that at this state deformation occurred in an open fluid–rock system. Link-up of shear veins led to the formation of the emergent fault slip surfaces which rapidly concentrated all the subsequent deformation.

In this faulting model, fault-related structures and rocks evolved from a closed system with fluid–rock equilibrium at depth to a more open system with limited influx of meteoric water in shallower conditions.

We especially thank D. Blamard (LSCE-Gif Sur Yvette) for the isotopes analysis and his help for data interpretation, M. Bussolotto (UPXI), J. Thibieroz (UPVI) and M. Pagel (UPXI) for their help with fluid inclusions analysis and interpretation, and J. P. Bilotte (UPXI) for making the thin sections. Thanks to A. McCaig and C. Wibberley whose comments helped to improve the manuscript.

References

AUBOIN, J. & DERCOURT, J. 1962. Zone préapulienne, zone ionienne et zone du Gavrovo en Péloponnèse occidental. *Bulletin de la Société Géologique, France*, **7**, 785–794.

BALLY, V. 2005. *Le mécanisme d'ouverture du rift de Corinthe, localisation d'un détachement et rôle de la Nappe des Phyllades.* Rapport Master II, Université de Paris VI, inédit.

BARTLETT, W. L., FRIEDMAN, M. & LOGAN, J. M. 1981. Experimental folding and faulting rocks under confining pressure, part IX. Wrench faults in limestone layers. *Tectonophysics* **79**, 255–277.

BENEDICTO, A., LABAUME, P., MICARELLI, L. & CARRIO, E. 2004. Deformation mechanisms in extensional fault propagation folding involving carbonate rocks: the Pyrgaki fault, Corinth rift (Greece). *In*: *Réunion des Sciences de la Terre, Poster Proceeding*. Société Geologique de France, Strasbourg.

BERNARD, P., LYON-CAEN, H. *ET AL*. 2006. Seismicity, deformation and seismic hazar in the western rift of Corinth: new insights from the Corinth Rift Laboratory (CRL). *Tectonophysics*, **426**, 7–30.

BODNAR, R. J. 1993. Revised equation and table for determining the freezing point depression of H2O-NaCl solution. *Geochimica et Cosmochimica Acta*, **57**, 683–684.

BOLES, J. R. & GRIVETTI, M. 2000. Calcite cementation along the Refugio/Carneros fault, Coastal California: a link between deformation, fluid movement and fluid–rock interaction at a basin margin. *Journal of Geochemical Exploration*, **69–70**, 313–316.

BRADBURY, H. J. & WOODWELL, G. R. 1987. Ancient fluid flow within foreland terrains. *In*: GOFF, J. C. & WILLIAMS, B. P. J. (eds) *Fluid Flow in Sedimentary Basins and Aquifers.* Geological Society of London. Special Publications, **34**, 87–102.

BROOKS, M. & FERENTINOS, G. 1984. Tectonics and sedimentation in the Gulf of Corinth and the Zakynthos and Kefallinia Channels, western Greece. *Tectonophysics*, **101**, 25–54.

CAUSSE, C., MORETTI, I., ESCHARD, R., MICARELLI, L., GHALEB, B. & FRANK, N. 2004. Kinematics of the Corinth Gulf inferred from calcite dating and syntectonic sedimentary characteristics. *Comptes Rendus Geoscience*, **336**, 281–290.

CELLO, G., INVERNIZZI, C., MAZZOLI, S. & TONDI, E. 2001. Fault properties and fluid flow patterns from Quaternary faults in the Apenines, Italy. *Tectonophysics*, **336**, 63–78.

CLARK, I. & FRITZ, P. 1997. *Environmental Isotopes in Hydrogeology*. CRC Press, Boca Raton, FL.

CRAIG, H., BOATO, G. & WHITE, D. E. 1956. *Isotopic Geochemistry of Thermal Waters.* US National Academy of Sciences and National Research Council, Pubications, **400**, 29–38.

COLLIER, R. E. L. 1990. Eustatic and tectonic controls upon Quaternary coastal sedimentation in the Corinth Basin, Greece, *Journal of Geological Society of London*, **147**, 301–314.

COLLIER, R. E. L., LEEDER, M. R., ROWE, P. J. & ATKINSON, T. C. 1992. Rates of tectonic uplift in the Corinth and Megara basins, central Greece. *Tectonics*, **11**, 1159–1167.

CORNET, F. H., DOAN, L. M., MORETTI, I. & BORM, G. 2004. Drilling through the active Aigion Fault: the AIG10 well observatory. *Comptes Rendus Geoscience*, **336**, 395–406.

DANIEL, J. M., MORETTI, I., MICARELLI, L., ESSAUTIER CHUYNE, S. & DELLE PIANE, C. 2004. Macroscopic structural analysis of AIG10 well (Gulf of Corinth, Greece). *Comptes Rendus Geoscience*, **336**, 435–444.

DART, C. J., COLLIER, R. E. L., GAWTHORPE, R. L., KELLER, J. V. A. & NICHOLS, G. 1994. Sequence stratigraphy of (?)Pliocene–Quaternary synrift, Gilbert-type fan deltas, northern Peloponnesus, Greece. *Marine and Petroleum Geology*, **11**, 545–560.

DERCOURT, J. 1964. *Contribution à l'étude géologique d'un secteur du Péloponnèse septentrional.* Thèse d'état, Université de Paris, *Annales Géologiques des Pays Helléniques*, **15**.

DE WEVER, P. 1975. *Etude géologique des séries apparaissant en fenêtre sous l'allochtone pindique (série de Tripolitza et série epimétamorphique de Zaroukla), Péloponnèse septentrional, Grèce.* Thèse 3ème cycle, Université de Lille, France, inédite.

DIA, A. N., COHEN, A. S., O'NIONS, R. K. & JACKSON, J. A. 1997. Rates of uplift investigated through 230Th dating in the Gulf of Corinth (Greece). *Chemical Geology*, **138**, 171–184.

DUFAURE, J. J. 1975. *Le relief du Péloponnèse.* Thèse d'état, Université Paris IV, France, inédite.

DUFAURE, J. J. 1977. *Carte géologique du Péloponnèse à 1/200.000*. CNRS-Institut de Géographie, Paris.

EXADAKTYLOS, G. E., VARDOULAKIS, I., STAVROPOULOU, M. C. & TSOMBOS, P. 2003. Analogue and numerical modelling of normal fault patterns produced due to slip along a detachment zone. *Tectonophysics*, **376**, 117–134.

FERENTINOS, G., BROOKS, M. & DOUTSOS, T. 1985. Quaternary tectonics in the Gulf of Patras, western Greece. *Journal of Structural Geology*, **7**, 713–717.

FLOTTÉ, N. 2003. *Caractérisation structurale et cinématique d'un rift sur détachement: le rift de Corinthe-Patras, Grèce.* Thèse de doctorat, Université Paris XI Orsay, France, Inédite.

FLOTTÉ, N. & SOREL, D. 2001. Structural cross-sections through the Corinth-Patras detachment fault-system in the northern Peloponnesus, Aegean Arc, Greece, *In*: *9th International Congress, XXXIV/1*, Athens, Greece. Bulletins of the Geological Society of Greece, Athens, 235–241.

FLOTTÉ, N., PLAGNES, V., SOREL, D. & BENEDICTO, A. 2001. Attempt to date Pleistocene normal faults of the Corinth-Patras Rift (Greece) by U/Th method, and tectonic implications. *Geophysical Research Letters*, **28**, 3769–3772.

GIURGEA, V., TRETTENMAIER, D., PIZZINO, L., UNKEL, I., HÖTZL, H., FÖSTER, A. & QUATTROCCHI, F. 2004. Preliminary hydrogeological interpretation of the Aegion area from the AIG10 borehole data. *Comptes Rendus Geoscience*, **336**, 467–475.

GOLDSTEIN, R. H. & REYNOLDS, T. J. 1994. *Systematic of Fluid Inclusions in Diagenetic Minerals.* Society of Economic Paleontologists and Mineralogists, Tulsa, Short Course **31**.

GOLDSWORTHY, M. & JACKSON, J. 2001. Migration of activity within normal fault systems: examples from the Quaternary of mainland Greece. *Journal of Structural Geology*, **23**, 489–506.

HENRY, P. & MORETTI, I. 2006. The understanding of fault activity from natural laboratories. *Tectonophysics*, **426**, 1–5.

JOHNSON, A. M. & FLETCHER, R. C. 1994. *Folding of Viscous Layers – Mechanical Analysis and Interpretation of Structures in Deformed Rock*. Columbia University Press, New York.

KIM, S. T. & O'NEIL, J. R. 1997. Equilibrium and nonequilibrium oxygen isotope effects in synthetic carbonates. *Geochimica Cosmochimica Acta*, **61**, 3461–3475.

LABAUME, P., BETTY, C. & LAURENT, P. 1991. Syndiagenetic evolution of shear structures in superficial nappes: an example from the Northern Apennines (NW Italy). *Journal of Structural Geology*, **13**, 385–398.

LABAUME, P., CARRIO-SCHAFFHAUSER, E., GAMOND, J. F. & RENARD, F. 2004*a*. Deformation mechanisms and fluid-driven mass transfers in the recent fault zones of the Corinth Rift (Greece). *Comptes Rendus Geoscience*, **336**, 375–383.

LABAUME, P., CARRIO-SCHAFFHAUSER, E. & TRAVÉ, A. 2004*b*. Fluid-driven mass transfer in recent normal fault zones of the Corinth Rift (Greece). Constraints from microstructural and geochemical analysis of calcite cements. *In*: *Réunion des Sciences de la Terre, Poster Proceeding*. Société Géologique de France, Strasbourg.

LEE, Y. L., MORSE, J. W. & WILTSCHKO, D. V. 1996. An experimentally verified model for calcite precipitation in veins. *Chemical Geology*, **130**, 203–215.

LEEDER, M. R., MCNEILL, L., COLLIER, R. E. L., PORTMAN, C., ROWE, P., ANDREWS, J. & GAWTHORPE, R. L. 2003. Corinth Rift margin uplift: new evidence from Late Quaternary marine shorelines. *Geophysical Research Letters*, **30**, 1611.

LE POURHIET, L. 2004. *Modélisation thermo-mécanique de l'extension continentale: développements théoriques et application au Golfe de Corinthe (Grèce).* Thèse de Doctorat, Université de Paris VI, inédite.

LE POURHIET, L., EVGENII, B. & MORETTI, I. 2004. Rifting through a stack of inhomegeneous thrusts (the dipping pie concept). *Tectonics*. **23**, TC4005.

LIN, A., TANAKA, N., UDA, S. & SATISH-KUMAR, M. 2003. Repeated coseismic infiltration of meteoric and seawater into deep fault zones: a case study of the Nojima fault zone, Japan. *Chemical Geology*, **202**, 139–153.

LYON-CAEN, H., PAPADIMITRIOU, P., DESCHAMPS, A., BERNARD, P., MAKROPOULOS, K., PACCHIANI, F. F. & PATAU, G. 2004. First results of the CRLN seismic network in the western Corinth Rift: evidence for old-fault reactivation. *Comptes Rendus Geoscience*, **336**, 343–351.

MAIR, K. & MARONE, C. 1999. Friction of simulated fault gouge for a wide range of velocities and normal stresses. *Journal of Geophyical Research*, **104**, 28 899–28 914.

MALARTRE, F., FORD, M. & WILLIAMS, E. A. 2004. Preliminary biostratigraphy and 3D geometry of the Vouraikos Gilbert-type fan delta, Gulf of Corinth, Greece. *Comptes Rendus Geoscience*, **336**, 269–280.

MICARELLI, L., MORETTI, I. & DANIEL, J. M. 2003. Structural properties of rift-related normal faults: the case study of the Gulf of Corinth, Greece. *Journal of Geodynamics*, **36**, 275–303.

MICARELLI, L., BENEDICTO, A., INVERNIZZI, C., SAINT-BEZAR, B., MICHELOT, J. L. & VERGÉLY, P. 2005. Influence of P/T conditions on the style of normal fault initiation and growth in limestones from the SE-Basin, France. *Journal of Structural Geology*, **27**, 1577–1598.

MORETTI, I., SAKELLARIOU, D., LYKOUSIS, V. & MICARELLI, L. 2003. The Gulf of Corinth: an active half graben? *Journal of Geodynamics*, **36**, 323–340.

MORSE, J. W. & MACKENZIE, F. T. 1993. Geochemistry of sedimentary carbonates: developments in sedimentology. *Geochimica et Cosmochimica Acta*, **57**, 2919–2920.

MUCHEZ, P., SLOBODNIK, M., VIAENE, W. A. & KEPENS, E. 1995. Geochemical constraints on the origin and migration of paleofluids in the northern margin of the Variscan foreland, southern Belgium. *Sedimentary Geology*, **96**, 191–200.

ORI, G. G. 1989. Geologic history of the extensional basin of the Gulf of Corinth (Miocene–Pleistocene), Greece. *Geology*, **17**, 918–921.

PI ALPARIN, J. M., MARTHELOT, J. M., GALVÉ, A., SACHPAZI, M., TAYLOR, B., LAIGLE, M. & HIRN, A. 2004. Seismic refraction imaging of the southern Corinth Rift shoulder at Derveni. *Comptes Rendus Geoscience*, **336**, 251–257.

PILI, E., POITRASSON, F. & GRATIER, J. P. 2003. Carbon–oxygen isotope and trace element constraints on how fluids percolate faulted limestones from the San Andreas Fault System: partitioning of fluid sources and pathways. *Chemical Geology*, **190**, 231–250.

PIRRIE, D. & MARSHALL, J. D. 1990. High-paleolatitude Late Cretaceous paleotemperatures: new data from James Ross Island, Antarctica. *Geology*, **18**, 31–34.

PIZZINO, L., QUATTROCCHI, F., CINTI, D. & GALLI, G. 2004. Fluid geochemistry along the Eliki and Aigion seismogenic segments (Gulf of Corinth, Greece). *Comptes Rendus Geosciences*, **336**, 367–374.

RENARD, F., GRATIER, J. P. & JAMTVEIT, B. 2000. Kinetics of crack-sealing, intergranular pressure solution, and compaction around active faults. *Journal of Structural Geology*, **22**, 1395–1407.

ROBERTS, G. & STEWART, I. 1994. Uplift, deformation and fluid involvement within an active normal fault zone in the Gulf of Corinth, Greece. *Journal of the Geological Society of London*, **151**, 531–541.

ROEDDER, E. 1984. *Fluid Inclusions*. Mineralogical Society of America.

SACHPAZI, M., CLÉMENT, C., LAIGLE, M., HIRN, A. & ROUSSOS, N. 2003. Rift structure, evolution, and earthquakes in the Gulf of Corinth, from reflection seismic images. *Earth and Planetary Science Letters*, **216**, 243–257.

SÉBRIER, M. 1977. *Tectonique récente d'une transversale à l'arc égéen. Le golfe de Corinthe et ses régions périphériques.* Thèse de 3ème cycle, Université Paris XI, Orsay, inédite.

SEGER, M. & ALEXANDER, J. 1993. Distribution of Plio-Pleistocene and modern coarse-grained deltas south of the Gulf of Corinth, Greece. *In*: FROSTICK, L. E. & STEEL, R. J. (eds) *Tectonic Controls and Signatures in Sedimentary Successions*. Association of Sedimentologists, Special Publications, **20**, 37–48.

SIBSON, R. H. 2000. Fluid involvement in normal faulting. *Journal of Geodynamics*, **29**, 469–499.

SOREL, D. 2000. A Pleistocene and still-active detachment fault and origin of the Corinth-Patras Rift, Greece. *Geology*, **28**, 83–86.

STEWART, I. & HANCOCK, P. L. 1988. Normal fault zone evolution and fault scarp degradation in the Aegean region. *Basin Research*, **1**, 139–153.

STEWART, I. S. & HANCOCK, P. L. 1990. Brecciation and fracturing within neotectonic normal fault zones in the Aegean region. *In*: KNIPE, R. J. & RUTTER, E. H. (eds) *Deformation Mechanisms, Rheology and Tectonics.* Geological Society, Special Publications, **54**, 105–112.

TRAVÉ, A., CALVET, F., SOLER, A. & LABAUME, P. 1998. Fracturing and fluid migration during Paleogene ompression and Neogene extension in the Catalan coastal ranges, Spain. *Sedimentology*, **45**, 1063–1082.

VITA-FINZI, C. & KING, G. C. P. 1985. The seismicity, geomorphology and structural evolution of the Corinth area of Greece. *Philosophical Transactions of the Royal Society of London*, **314**, 379–407.

WESTAWAY, R. 2002. The Quaternary evolution of the Gulf of Corinth, Central Greece: coupling between surface processes and flow in the lower continental crust. *Tectonophysics*, **348**, 269–318.